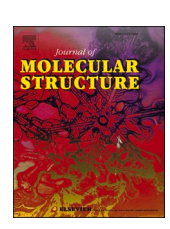
ELSEVIER

Contents lists available at ScienceDirect

Journal of Molecular Structure

journal homepage: www.elsevier.com/locate/molstr



Pyrene carbaldehyde Schiff base as multifunctional chemosensors for environmental thorium determination and its real-time applications

Prabhu Viswanathan ^a, Chandra Sureshkumar ^{a,*}, A. Asrar Ahamed ^b, Govindasamy Siva ^c, Michael Benjamin ^{d,*}

ARTICLE INFO

Keywords: Thorium Fluorescence Pyrene 8-Hydroxyquinoline Carbohydrazide

ABSTRACT

Thorium (Th^{4+}) sensing is critical to nuclear fuel cycle monitoring and safeguards since it may become a fissile material after neutron irradiation. Detection and assessment of Th^{4+} ions contamination is also crucial for environmental monitoring. Herein, a new pyrene-based fluorescent probe was developed by incorporating an 8-hydroxyquinoline moiety into the pyrene fluorophore (HQ-PY), which is used for Th^{4+} ions detection via fluorescent quenching in semi-aqueous media. An on-off monomer-excimer conversion of HQ-PY was achieved through the formation of a 2:1 coordination complex and fluorescent quenching at 520 nm. The HQ-PY exhibited excellent selectivity, high sensitivity (LOD = 1.8 nM), and rapid response (55 s) to Th^{4+} ions. HQ-PY binding to Th^{4+} ions was investigated by Th^{4+} Th^{4+} Th^{4+} in the experimental data further supplemented by density functional theory-based computational calculations. Furthermore, we extended this probe performance in real water samples and monazite sand samples to monitor and quantify the pollution caused by Th^{4+} ions.

1. Introduction

The detection of heavy metal ions is crucial due to the significant environmental and health risks posed by their abnormal concentrations. Among these, thorium (Th⁴⁺) stands out as a highly radioactive heavy metal ion, commonly utilized as a nuclear reactor fuel and in industrial applications such as alloy production, welding equipment, and optical lenses [1,2]. Naturally ubiquitous in trace amounts across environmental matrices, including rocks, soil, water, and biological organisms, thorium poses serious health threats when accumulated in the body [3]. Several studies indicate that prolonged exposure through inhalation of radioactive dust or bioaccumulation can lead to chronic conditions such as lung, pancreatic, and bone cancers [4]. These risks underscore the critical need for advancing sensitive and selective detection techniques capable of identifying Th⁴⁺ at micromolar concentrations, a persistent challenge in environmental monitoring and public health protection [5]. Current methodologies for Th⁴⁺ ions detection include inductively

coupled plasma-optical emission spectrometry (ICP-OES) and inductively coupled plasma-mass spectrometry (ICP-MS), often coupled with ion chromatography for enhanced specificity. Additional approaches such as neutron activation analysis, alpha spectrometry, gamma spectrometry, spectrophotometry, and spectrofluorimetry are also employed depending on sample characteristics and required sensitivity. While ICP-MS offers high precision, its effectiveness is constrained by factors like column capacity, sample acidity, and matrix interferences, which can skew results. Furthermore, many techniques necessitate extensive sample preparation, including preconcentration and separation steps, to mitigate low analyte concentrations or competing ions [6-11]. These preparatory stages not only prolong analysis time but also introduce potential errors, highlighting the need for streamlined protocols in thorium detection [12]. Using gamma spectrometry, it is possible to determine their decay products directly. Despite this, it takes some time for radiochemical equilibrium to be established between the decay products.

E-mail addresses: chandra@psgcas.ac.in (C. Sureshkumar), sweetbenjam@gmail.com (M. Benjamin).

^a Department of Chemistry, PSG College of Arts and Sciences, Coimbatore, 641 014, India

^b PG and Research Department of Chemistry, Jamal Mohamed College (Autonomous), Affiliated to Bharathidasan University, Tiruchirappalli, 620020, Tamil Nadu, India

^c Department of Physics, Bannari Amman Institute of Technology, Sathyamangalam, 638 401, Tamil Nadu, India

d Department of Biomaterials, Saveetha Dental College and Hospital, Saveetha Institute of Medical and Technical Sciences (SIMATS), Saveetha University, Chennai, 600 077, India

^{*} Correspondence authors.

Scheme 1. Synthetic route of probe HQ-PY.

The fluorescence technique has several advantages over other techniques, including its acceptable selectivity and sensitivity, as well as its inexpensive and rapid procedures for detecting metal ions [13]. The fluorescence technique has been one of the potential sensing techniques in recent decades [14–16]. A significant challenge, however, remains the lack of a turn-off fluorescence sensor for Th^{4+} ions in an aqueous solution despite this technique's sensitivity and selectivity [5]. To construct a basic ionic fluorescent sensor, two intramolecularly linked functional units have to be combined: ionophores with metal-chelating structures are designed to recognize and bind specific target ions, and a fluorogenic unit as a readout part whose photophysical properties are perturbed during binding [17–20].

Here, we have synthesized a pyrene-based probe (HQ-PY) linked to an 8-hydroxy-2-quinolinecarbohydrazide moiety via a Schiff-base linkage. As a fluorophore, the pyrene part of the synthesized compound would act as a fluorescent reporter, while the 8-hydroxy-2-quinolinecarboxyhydrazide part, containing the 8-hydroxyquinoline unit, would serve as a chelating agent. As a result, it is an ideal compound for the detection of cations. As expected, it has been demonstrated to be a selective Th⁴⁺ sensor through spectrophotometric and spectrofluorometric studies using a variety of cations.

2. Experimental section

The detailed instrumentation, chemical resource, solution preparation, and computational methods are provided in the supporting information.

2.1. Synthesis of probe

The 1-pyrene carboxaldehyde (PY-CHO) (232 mg, 1.01 mmol) and 8-hydroxy-2-quinoline carbohydrazide (HQ-HY) (420 mg, 1.01 mmol)

were dissolved in 20 mL of ethanol. Few drops of glacial acetic acid were added to the above solution and refluxed for two hours. The reaction mixture was cooled to room temperature, and the precipitates were collected via filtering. The filtered material was purified by crystallization in acetonitrile, yielding a bright golden-yellow solid (HQ-PY). Characterization ($C_{27}H_{17}N_{3}O_{2}$) HQ-PY: FTIR (ATR, cm $^{-1}$): 3566 (V_{-OH}), 3256 (V_{-NH}), 3065 (V_{-CH}), 1670 ($V_{-C=O}$), 1601 ($V_{-CH=N}$), 1530 ($V_{-C=N}$). ^{1}H NMR (400 MHz, DMSO- d_{6} , δ , ppm): 12.81 (s, 1H), 10.27 (s, 1H), 9.67 (s, 1H), 9.01 (d, 1H), 8.66 (d, 1H), 8.42 (d, 1H), 8.40 (m, 4H), 8.30 (m, 3H), 8.16 (t, 1H), 7.65 (d, 1H), 7.55 (d, 2H), 7.27 (d, 1H). ^{13}C NMR (100 MHz, DMSO- d_{6} , δ , ppm): 160.53, 154.14, 148.24, 147.28, 138.66, 136.87, 132.62, 131.35, 130.64, 130.36, 130.27, 129.39, 129.25, 129.07, 127.91, 127.30, 127.17, 126.71, 126.36, 125.95, 125.78, 124.66, 124.24, 123.20, 119.69, 118.29, 112.48. HR-MS [M+H] $^+$: calculated 416.1394 and obtained 416.1399.

3. Results and discussions

The synthesis began with the preparation of 8-hydroxy-2-quinoline-carbohydrazide (HQ-HY) following previously reported methods [11]. Subsequently, the Schiff base probe HQ-PY was obtained by reacting HQ-HY with PY-CHO under standard Schiff base reaction conditions, as illustrated in Scheme 1. The purified HQ-PY product was thoroughly characterized using ¹H-NMR, ¹³C-NMR, FT-IR, and HR-MS analyses (Fig. S1–S4). In the ¹H NMR spectrum, signals observed at 12.81, 10.27, and 9.67 ppm correspond to the –NH proton, –OH proton, and the imine (–CH=N) proton, respectively. The FT-IR spectrum exhibited characteristic absorption bands at 3566, 3256, 1670, and 1601 cm⁻¹, confirming the presence of –OH, –NH, C=O, and CH=N functional groups. These spectroscopic data confirm the successful synthesis and structural integrity of the HQ-PY probe.

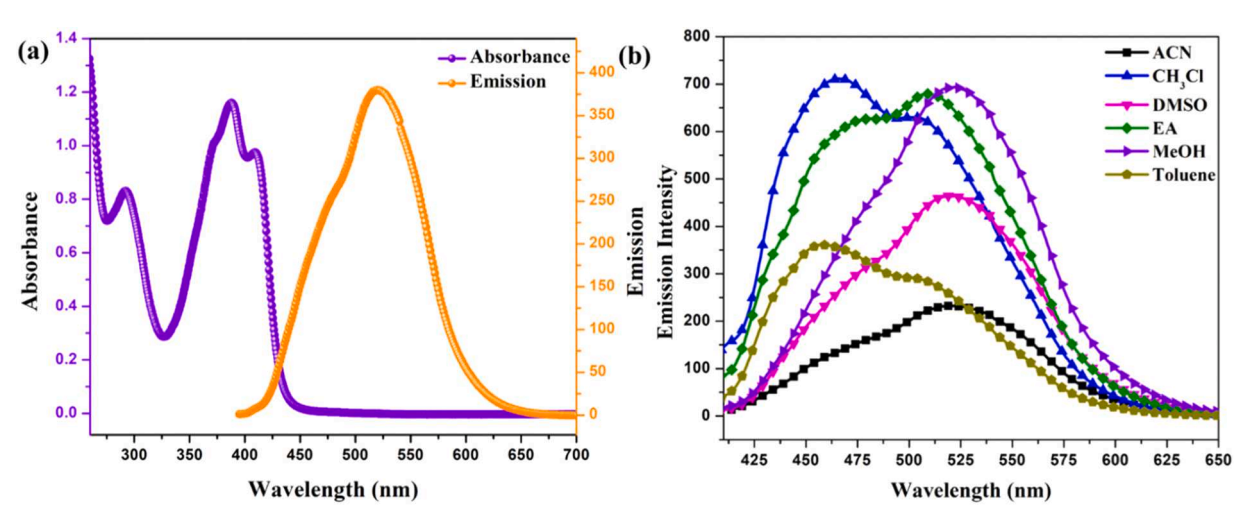


Fig. 1. (a) UV-Vis absorbance and fluorescence emission spectra of HQ-PY in DMSO solvent. (b) The emission spectral change of HQ-PY in various solvents.

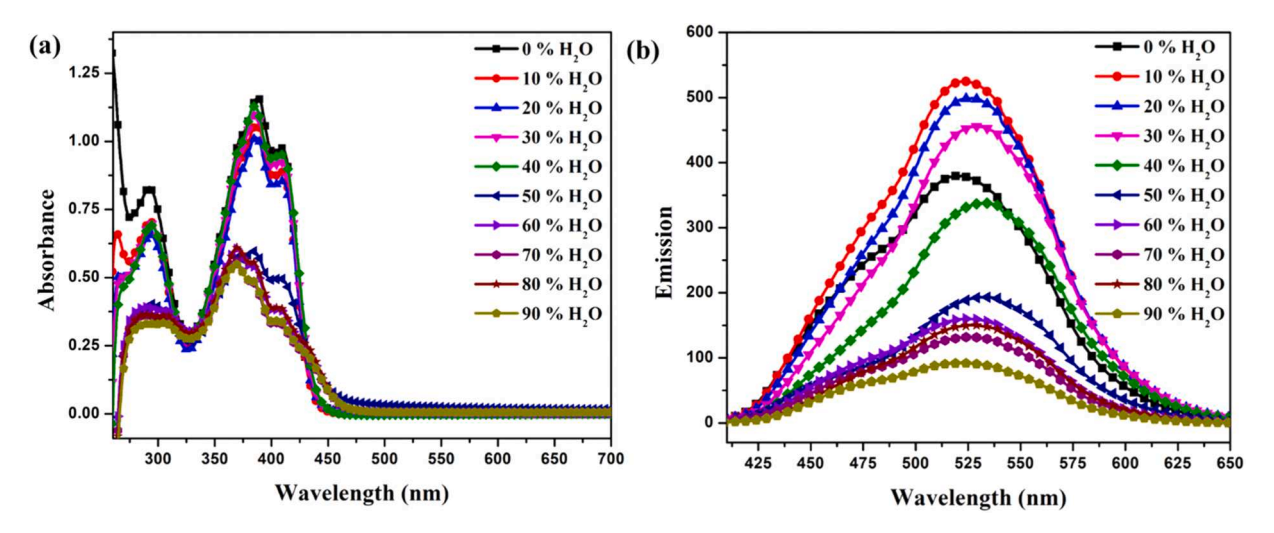


Fig. 2. (a) UV-Vis absorbance and (b) emission spectral change of probe HQ-PY with various water contents in DMSO.

3.1. Solvent effect

The UV-Vis absorption and fluorescence emission spectra of HQ-PY (30 μ M) were recorded in DMSO solvent, as shown in Fig. 1a. In DMSO, HQ-PY displayed three prominent absorption bands centered at 290 nm, 388 nm, and 410 nm. The short absorption band at 290 nm with a molar absorbance coefficient (ε) of 2.79 \times 10⁴ L.mol⁻¹.cm⁻¹ is attributed to $\pi \rightarrow \pi^*$ transitions within the conjugated aromatic system of the pyrene core. The broader band from 325 to 450 nm centered at 388 nm with an ε of 3.90 \times 10⁴ L.mol⁻¹.cm⁻¹ arises from $n\rightarrow\pi^*$ transitions involving non-bonding electrons from heteroatoms (such as nitrogen or oxygen), strong π -conjugation and possible charge-transfer interactions across the HQ-PY system. Similarly, the emission spectra of HQ-PY were found at 520 nm upon excitation at 388 nm in DMSO solvent. To investigate the solvatochromic behavior of HQ-PY, its absorbance and emission spectra were recorded in various solvents with different polarities. The results show that distinct broader dual absorption bands range from 488 nm to 410 nm (Fig. S6). When excited at 388 nm, HQ-PY exhibited a fluorescence emission peak at 520 nm in DMSO. Notably, the maximum fluorescence emission experienced a redshift of 43 nm, shifting from 458 nm in toluene to 520 nm in DMSO, indicating significant sensitivity to solvent polarity. Correspondingly, the Stokes shift ranged from 4378 to 6719 cm⁻¹ as solvent polarity increased (**Table S1**).

While absorption solvatochromism was minimal, pronounced bathochromic shifts were observed in the emission spectra, highlighting the influence of solvent relaxation on fluorescence characteristics. The substantial Stokes shift and strong solvatochromic response make HQ-PY a promising candidate for chemosensor and bioimaging applications, where such properties are highly desirable.

3.2. Aggregation study

Aggregation-induced emission (AIE) may also be responsible for the enhancement of fluorescence, as aggregation inhibits the rotation of molecules. As shown in Fig. 2a and 2b, both UV-Vis absorbance and emission intensity did not significantly change until 30% water fraction in DMSO; thereafter, the fluorescence intensity decreased, indicating that aggregation causes quenching (ACQ). It may be because HQ-PY presents pyrene rings that aggregate, thereby facilitating stacking and AIE activity. This study also confirms that up to 30% water on DMSO, both the UV-Vis absorbance and emission intensity of probe HQ-PY did not change, beyond this level there a change was observed. This indicates that the optimum water tolerance of up to 30% on DMSO will be carried out for further studies.

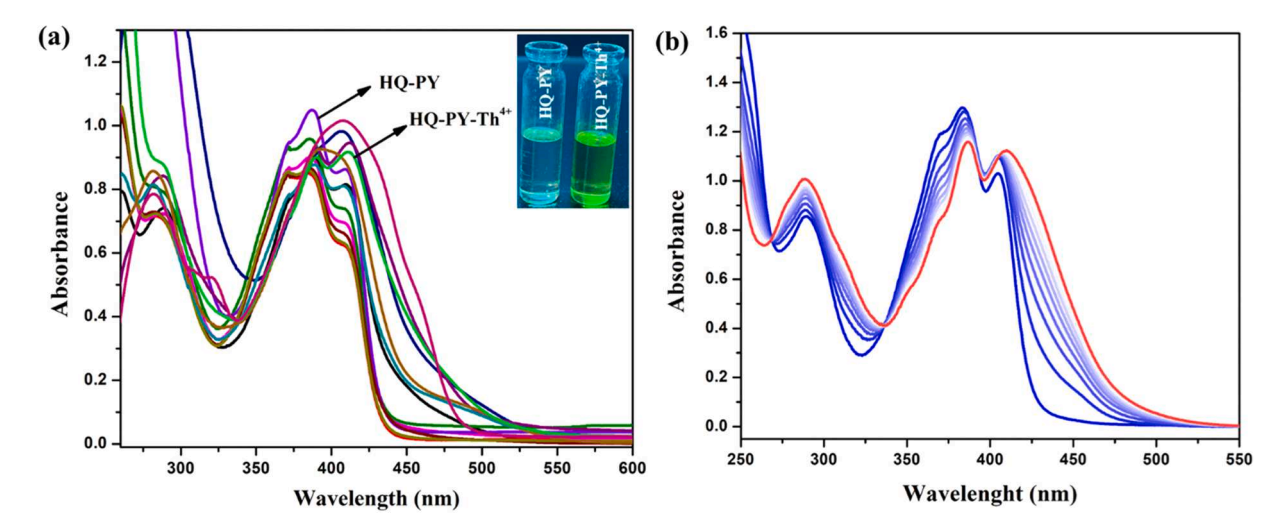


Fig. 3. (a) UV-Vis absorbance spectral change of probe HQ-PY in the presence and absence of various metal ions [Insert: Visual color change of HQ-PY, HQ-PY-Th⁴⁺ under normal light]. (b) UV-Vis absorbance spectral change of probe HQ-PY with increasing concentration of Th⁴⁺ ions in DMSO: HEPES (7:3, v/v).

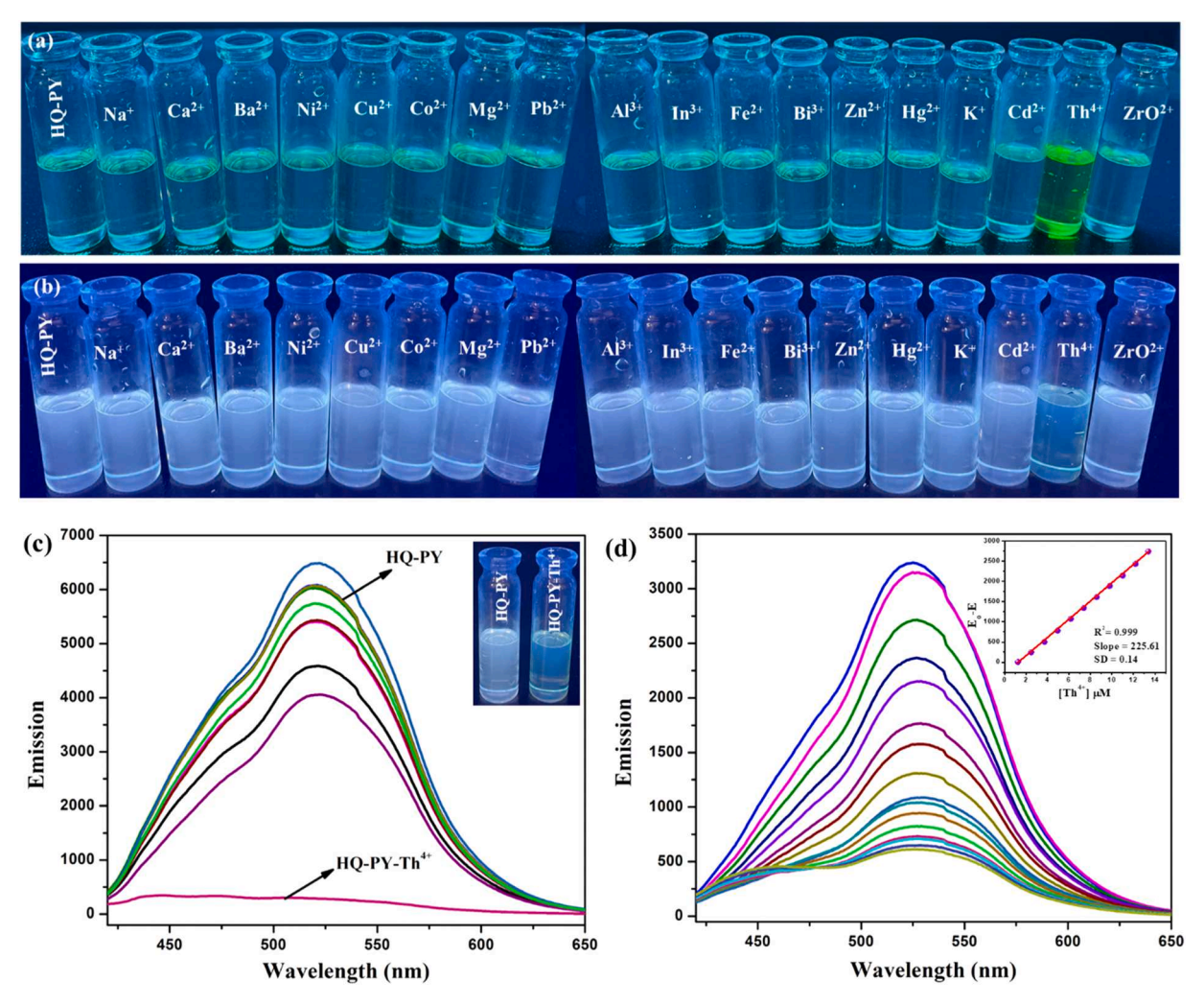


Fig. 4. (a, b) The visual color change images of probe HQ-PY in the presence and absence of metal ions under daylight and UV-light. (c) Emission spectral change of probe HQ-PY in the presence and absence of various metal ions. (d) Emission spectral change of probe HQ-PY with incremental addition of Th⁴⁺ ions. Insert: calibration curve ($\lambda_{ex} = 388$ nm) in DMSO: HEPES (7:3, v/v).

3.3. Spectrophotometry and spectrofluorometric studies

The spectral properties of probe HQ-PY were investigated in a DMSO: HEPES (7:3, v/v) solution at room temperature. To evaluate its cation sensing capabilities, UV-Vis absorption and emission spectra were analyzed upon introducing various metal cations, including Cu^{2*} , Ni^{2*} , Th^{4*} , Co^{2*} , Mg^{2*} , Ag^* , Zn^{2*} , Al^{3*} , In^{3*} , Fe^{2*} , Pb^{2*} , Ca^{2*} , Bi^{3*} , Ba^{2*} , Hg^{2*} , Cd^{2*} , Na^* , and K^* ions. Distinctive changes were observed specifically with Th\$^{4*} ions: the free probe's dual absorption bands at 384 nm and 405 nm exhibited a slight redshift to 388 nm and 410 nm, respectively, while

other cations induced only minor spectral alterations (Fig. 3a). During absorbance spectral titration with Th⁴⁺ ions, the intensity of the original absorption bands progressively diminished, accompanied by the emergence of new peaks at 388 nm and 410 nm (Fig. 3b). This spectral shift correlated with a visible colorimetric transition from pale yellow to light green, consistent with the 5 nm redshift. The presence of sharp isosbestic points at 268 nm and 336 nm confirmed a well-defined equilibrium between the free probe HQ-PY and its Th⁴⁺ ions complex, indicating a single-step binding interaction.

The emission profile of probe HQ-PY in DMSO: HEPES (7:3, v/v)

Scheme 2. Proposed complexing of **HQ-PY** with Th⁴⁺ ions.

 Table 1

 Comparison of sensing parameters of the present probe with literature reports.

S. No	Structure Probe	Method	$\lambda_{abs} / \lambda_{em}$ (nm)	P: Th ⁴⁺	Ka (M ⁻	LOD (nM)	Medium	Applications	Ref.
1	N N N N N N N N N N N N N N N N N N N	Turn-ON FL	314/ 446	1:1	4.5 × 10 ⁴	4.9	CH ₃ CN/H ₂ O (50: 50, v/v)	Water sample analysis	[25]
2	он ОН	Turn-ON FL	300/600	2:1	-	56	EtOH/ Water (3:7, v/v)	Water sample analysis	[26]
3	OH	Turn-ON FL	360/ 445	2:1	6.79 × 10 ⁶	34	CH ₃ CN/ H ₂ O (9:1, v/v)	Water sample analysis	[27]
4	OH O Bu	Turn-ON FL	315/ 486	2:1	2.66 × 10 ⁴	1.1	PVC optode in $\rm H_2O$	Water sample analysis	[28]
5	OH O O HO	Turn-ON FL	360/530	1:1	-	34	CH ₃ OH/ H ₂ O (2:8 v/v)	Water sample analysis	[29]
6	N HO HO	Ratiometry FL	430/ 500	2:1	$6.68 \\ \times 10^4$	48.7	CH ₃ CN/ H ₂ O (8:2, v/v)	C. elegans Imaging	[17]
7	N N N N N N N N N N N N N N N N N N N	Turn-Off FL	430/ 475	2:1	$\begin{array}{c} 1.92 \\ \times 10^8 \end{array}$	18.7	CH ₃ CN/ H ₂ O (8:2, v/v)	C. elegans Imaging	[30]
8	N ₃ N NNNNNNNNNNNNNNNNNNNNNNNNNNNNNNNNNN	Ratiometry FL	400/ (550/ 585)	2:1	-	81	THF/ H ₂ O (1:9, v/ v)	Water sample analysis and Zebrafish imaging	[31]
9	HO HO OH	Turn-On FL	374/ 455	2:1	9.97 ×10 ⁹	7.19	EtOH/ H ₂ O (1:1, v/v)	Water sample analysis	[32]
10	OH OH	Turn-Off FL	388/ 520	2:1	1.70 × 10 ⁴	1.8	DMSO: HEPES (7:3, v/v)	Water sample analysis	Present Work

showed a distinct fluorescence band at 520 nm when excited at 388 nm. To evaluate the sensor's selectivity, various cations-including Cu²+, Ni²+, Th⁴+, Co²+, Mg²+, Ag*, Zn²+, Al³+, In³+, Fe²+, Pb²+, Ca²+, Bi³+, Ba²+, Hg²+, Cd²+, Na⁺, and K⁺-were introduced into the probe solution (Fig. 4a, b). Strikingly, Th⁴+ ions triggered near-complete quenching of the emission band at 520 nm, while other cations caused only marginal intensity fluctuations (Fig. 4c). During the fluorescence spectral titration with Th⁴+ ions, a gradual quenching of the emission intensity was observed over time. After the spectra stabilized, Th⁴+ ions were added incrementally, resulting in additional quenching of the emission band at 520 nm.

This quenching effect continued until it reached saturation with the addition of 0.5 equivalents of Th⁴⁺ ions (Fig. 4d). It was experienced without a doubt that the selectivity of the probe HQ-PY for Th⁴⁺ is great. Probe HQ-PY exhibited strong fluorescence due to monomer and hexamer formation and chelation-enhanced fluorescence quenching (CHEQ) [21,22]. Upon interaction with Th⁴⁺ ions, complex formation likely occurs at the nitrogen donor site, triggering a photo-induced electron transfer (PET) process from the nitrogen atoms in the imine bond to the pyrene ring. This PET mechanism results in a significant quenching of fluorescence intensity, as illustrated in Scheme 2. The

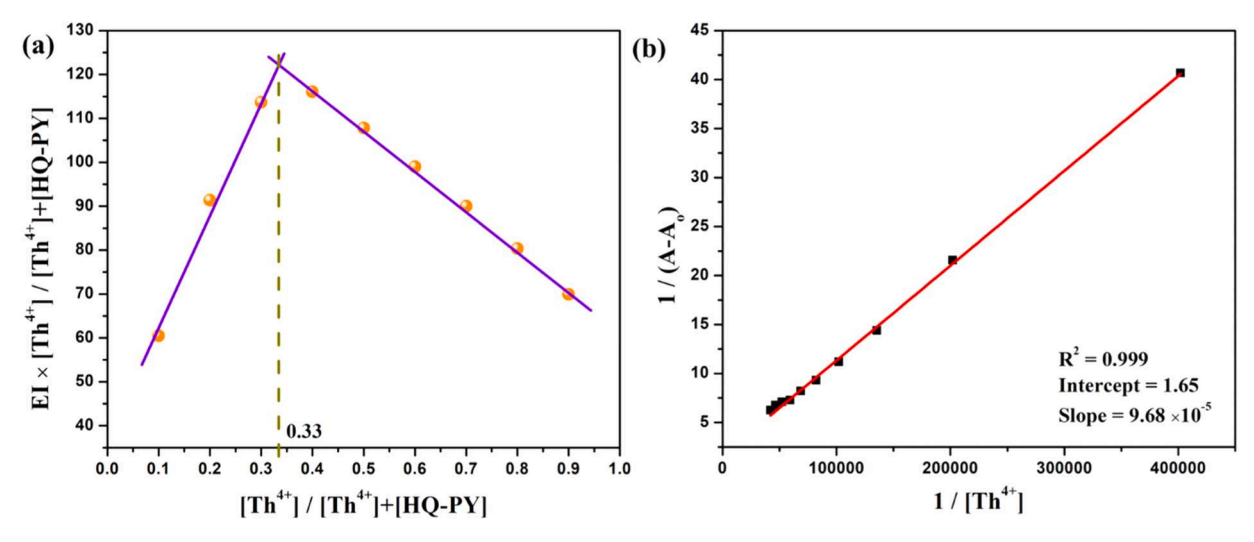


Fig. 5. (a) Job's plot (b) B-H plot for probe HQ-PY with Th⁴⁺ ions ($\lambda_{ex} = 388$ nm) in DMSO: HEPES (7:3, v/v).

detection limit (3 σ /S) of the HQ-PY probe was determined from the calibration curve plotting emission intensity against concentration at 520 nm (Fig. 4c) [23]. The probe exhibited a detection limit of 1.8 nM, which is significantly lower than the EPA's permissible limit of approximately 13 μ M. Compared to other reported turn-on/off Th⁴⁺ ion probes listed in Table 1, HQ-PY demonstrates a moderately good detection limit, highlighting its potential for sensitive detection of Th⁴⁺ ions. The optimal time response of HQ-PY with Th⁴⁺ ions was found to be 55s (Fig. S7).

Based on a Job's plot [24] experiment the binding stoichiometry between probe HQ-PY and Th4+ ions was determined by plotting the difference in emission intensity between the bound and free forms of the probe at 520 nm as a function of the mole fraction of Th⁴⁺ ions (Fig. 5a). In this experiment, the total molar concentration of both the probe (HQ-PY) and Th⁴⁺ ions were kept constant at 25 μM. In the resulting Job's plot, the breakpoint corresponds to the mole fraction of Th4+ ions present in the Th4+: HQ-PY complex. The stoichiometry of the complex can thus be expressed as cation: HQ-PY in the ratio $[\gamma_{Th}^{4+}n:(1-\gamma_{Th}^{4+})]$, where χ_{Th}^{4+} represents the mole fraction of Th⁴⁺ ions, calculated as the ratio of the concentration of Th4+ to the total molar concentration of both the probe and the cation. In our study, the inflexion point was found to be at $\chi Th^{4+} = 0.33$. From this inflection point, the stoichiometry of the Th⁴⁺: HQ-PY complex, as calculated, is 1:2. The molar fraction at the point of inflection represents the binding stoichiometry of HQ-PY+Th⁴⁺. The binding constant (Ka) of the probe HQ-PY with Th⁴⁺ was evaluated by the method of the Benesi-Hildebrand (B-H) equation for a 1:2 complex. The binding constants can be calculated from the slope of the plot of 1/A-A₀ as a function of 1/[Th⁴⁺], where A and A₀ are the absorbance intensity of probe HQ-PY in the absence of Th⁴⁺ ions, at an intermediate concentration, and a concentration of complete saturation with Th⁴⁺, respectively. As shown in Fig. 5b, the analysis yielded a binding constant of $1.70 \times 10^4 \, M^{-2}$, confirming a strong affinity between the probe and Th4+ ions. This quantitative validation aligns with the observed stoichiometry and underscores the probe's HQ-PY efficacy in forming stable complexes with Th4+ ions.

The effect of pH on the emission intensity of probe HQ-PY in the presence or absence of ${\rm Th}^{4+}$ ions was investigated. In this, the emission spectra were recorded in various pH buffers upon excitation at 388 nm. As shown in Fig. S8, the free probe shows intense maximum emission in the pH range from pH 5.0 to 8.0; below and above this pH range, the emission intensity was reduced due to the pH influence on the emission quenching. Further, upon the addition of ${\rm Th}^{4+}$ ions, this emission intensity was quenched to a minimum, which indicates the optimum pH range between 5.0 to 8.0 for further investigations.

The high selectivity of probe HQ-PY for Th⁴⁺ competition was

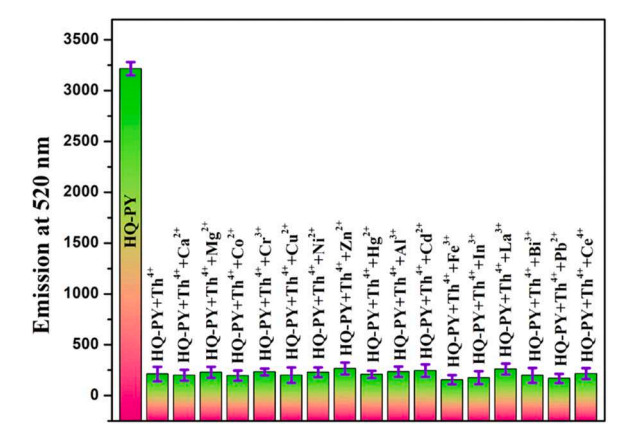


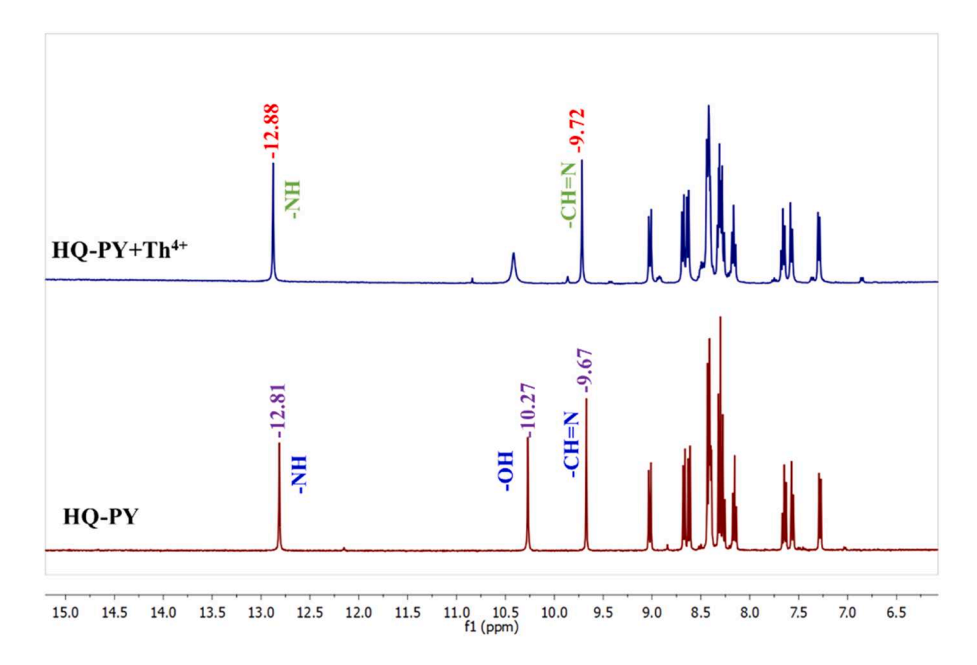
Fig. 6. (a) Emission intensity changes of probe HQ-PY with Th⁴⁺ ions in the presence of 10 equiv. of other metal ions ($\lambda_{ex}/\lambda_{em}=388/520$ nm) in DMSO: HEPES (7:3, v/v).

further verified by emission studies in which 10 equivalents of each cation were added once to 30 μM of probe HQ-PY, followed by 0.5 equivalents of Th^{4+} ions once each. Probe HQ-PY is very selective for Th^{4+} ions, as evidenced by the observation of changes in emission intensity at 520 nm and the retention of enhancement caused by Th^{4+} ions in the presence of other coexisting ions. Further, the reversible spectral changes of probe HQ-PY with Th^{4+} ions were investigated by using the strong chelating agent EDTA. As shown in Fig. S9, the free probe shows strong emission intensity at 520 nm was quenched with the addition of 0.5 equiv. of Th^{4+} ions. Then, into this solution, EDTA was added, as a result of EDTA- Th^{4+} complex formation, the free probe HQ-PY was found by strong emission intensity. Then this was further quenched with Th^{4+} ions added. This indicates that the present probe was reversible.

3.4. Binding mechanism study

The ¹H NMR was performed to investigate the reversible decomplexation/complexation mechanism of probe HQ-PY induced by Th⁴⁺ ions (Scheme 2). As shown in Fig. 6a, the addition of Th⁴⁺ ions caused substantial variations in the spectra. As a result of the addition of Th⁴⁺ ions, the upfield shifts of -NH, -OH, and -CH=N were observed, suggesting that probe HQ-PY binds specifically to Th⁴⁺ ions via its hydrazone and hydroxyl moieties (Fig. 7a).

The FT-IR spectrum of the free probe HQ-PY displays distinct vibrational bands at 3499 cm $^{-1}$ ($\nu_{-OH}),~3195~cm ^{-1}$ ($\nu_{-NH}),~1625~cm ^{-1}$



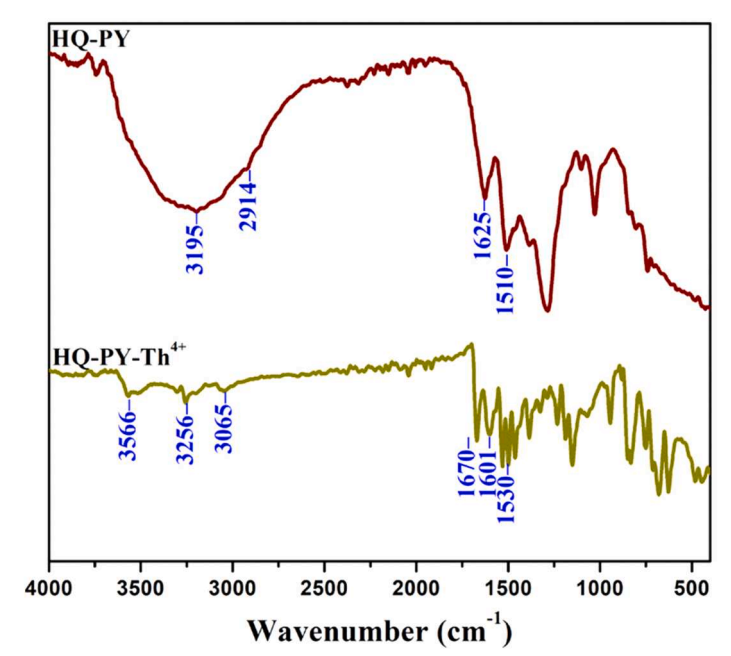


Fig. 7. (a) ¹H NMR spectral change of probe HQ-PY with Th(NO₃)₄.5H₂O in DMSO-d₆. (b) FTIR spectral change of probe HQ-PY and its Th⁴⁺ complex in ATR mode.

 $(\nu_{\text{-C=O}}),$ and 1510 cm⁻¹ $(\nu_{\text{-C=N}})$ (Fig. 7b). Upon complexation with Th⁴⁺ ions, the corresponding FT-IR spectrum reveals bands at 3566 cm⁻¹ $(\nu_{\text{-H}_2O}),$ 3256 cm⁻¹ $(\nu_{\text{-NH}}),$ 1670 cm⁻¹ $(\nu_{\text{-C=O}}),$ and 1530 cm⁻¹ $(\nu_{\text{-C=N}})$ (Fig. S5). These subtle shifts in the stretching frequencies of the –OH, –NH, C=O (amide), and C=N (imine) groups indicate their participation in the binding and complexation process with Th⁴⁺, as illustrated in Scheme 2. The ESI-mass spectral analysis shows the mass peak at 1060.1533, which corresponds to the involvement of the calculated mass corresponding to [2HQ-PY-2H+Th+H] (Fig. S5). This also further confirms the formation of a 2:1 stoichiometry complex between HQ-PY and Th⁴⁺ ions.

3.5. Computational study

The density functional theory (DFT) calculations of HQ-PY and HQ-PY-Th $^{4+}$ complexes were carried out using the basis sets B3LYP/6-31 G (d,p) and B3LYP/6-31(d,p)/SDD (ECP). HQ-PY and HQ-PY-Th $^{4+}$

complexes were optimized in terms of their geometry and orbital energy for the highest occupied molecular orbital (HOMO) and the lowest unoccupied molecular orbital (LUMO). HQ-PY illustrated in Fig. 8a illustrates that HOMO's electron density is largely distributed on the pyrene backbone, while LUMO's electron density is predominantly distributed on the pyrene backbone and the hydrazone moiety. As shown in Fig. S10, the electrostatic potential mapping on the van der Waals surface of HQ-PY is presented. The dominant electron distribution in the HQ-PY-Th⁴⁺ complex was centered on the pyrene moiety at HOMO, while electrons at LUMO were predominantly located in the metal center, suggesting a strong metal-to-ligand charge transfer process from the pyrene moiety to the Th⁴⁺ ions. To account for the redshift in absorption spectra caused by the lower HOMO-LUMO energy gap of HQ-PY-Th⁴⁺ ($\Delta E = 2.37$ eV) compared to the free probe HQ-PY ($\Delta E = 3.15$ eV), there may be some be seen in correlation. Additionally, HQ-PY's total energy decreased significantly after complexation with Th⁴⁺, indicating that the formed complex was extremely stable, which could

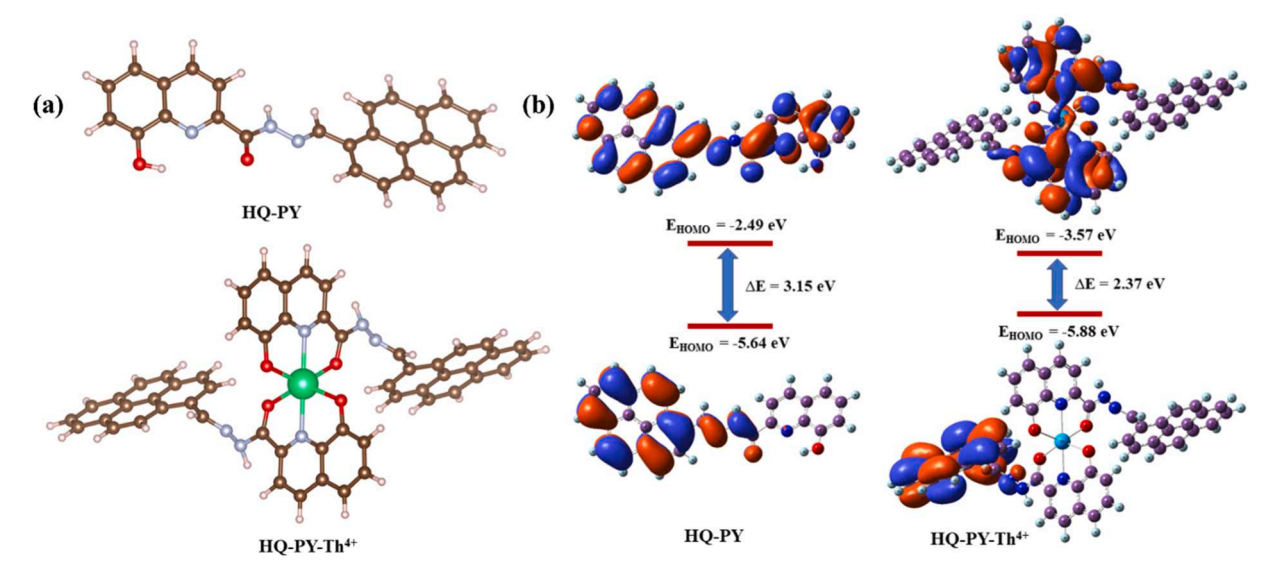


Fig. 8. (a) Optimized molecular geometry and its (b) FMO orbitals of probe HQ-PY and its Th⁴⁺ complex using DFT/B3LYP methods.

Table 2 Analytical performance of probe HQ-PY.

System	Th ⁴⁺ Added (μM)	Th ⁴⁺ found (μM)	Recovery (%)	RDS
Tap water	10	9.63	96.3	2.34
	20	19.24	96.2	2.01
DD Water	10	9.82	98.2	1.84
	20	19.76	98.8	1.53
Monazite sand	**	21.34	-	2.46

account for the spectral result as a result of CHEQ. According to the theoretical calculation above, the experimental response mechanism was in agreement with the theoretical calculation. By calculating the individual energies of the probe, the metal ion, and the resulting complex, the interaction energy for the HQ–PY–Th $^{4+}$ complex was found to be -915.023 kcal/mol. This strongly negative interaction energy not only confirms the remarkable stability of the complex but also aligns well with the high binding constant observed in the B-H analysis. The more negative the interaction energy, the greater the stability, further supporting the strong affinity between HQ-PY and Th $^{4+}$ ions.

3.6. Analytical applications

To evaluate the detection capability of the probe HQ-PY in practical applications, different types of water samples and monazite sand samples were evaluated for their detection of $\rm Th^{4+}$ ions. Based on the results shown in Table 2, it can be concluded that HQ-PY is capable of detecting environmental $\rm Th^{4+}$ ions in real samples. As a result of the standard addition method, each sample was spiked with specific amounts of $\rm Th^{4+}$, with excellent recovery rates of Th^4+ ions ranging from 96% to 101% in real samples, with a relative standard deviation of less than 3.57%, demonstrating the accuracy and applicability of HQ-PY in the detection of Th^4+ ions.

4. Conclusion

Herein, HQ-PY is a novel fluorescence probe developed by incorporating 8-hydroxyquinolone carbohydrozide into the pyrene fluorophore, which exhibits a specific turn-off fluorescent response towards Th^{4+} ions in DMSO: HEPES (7:3, v/v). HQ-PY displayed excellent selectivity, high sensitivity (LOD = 1.8 nM), rapid response (55 s), and a wide linear range. Through $^1\mathrm{H}$ NMR, FTIR, and ESI-Mass analysis, the binding

mechanism of HQ-PY with Th⁴⁺ ions was studied, and the experimental data were complemented by DFT calculations. Furthermore, we extended this probe performance in real water samples and monazite sand samples to monitor and quantify the pollution caused by Th⁴⁺ ions. As a result, this study is crucial to developing a sustainable strategy for monitoring and quantifying Th⁴⁺ ions pollution.

CRediT authorship contribution statement

Prabhu Viswanathan: Writing – original draft, Software, Methodology, Data curation. **Chandra Sureshkumar:** Writing – review & editing, Writing – original draft, Methodology, Data curation, Conceptualization. **A. Asrar Ahamed:** Software, Formal analysis, Data curation. **Govindasamy Siva:** Software, Formal analysis, Data curation. **Michael Benjamin:** Writing – review & editing, Supervision, Methodology, Investigation.

Declaration of competing interest

The authors declare that they have no known competing financial interests or personal relationships that could have appeared to influence the work reported in this paper.

Supplementary materials

Supplementary material associated with this article can be found, in the online version, at doi:10.1016/j.molstruc.2025.143500.

Data availability

Data will be made available on request.

References

- [1] A.K. Nayak, B.R. Sehgal, Thorium—Energy for the Future, Springer, 2019.
- [2] T. Moeller, G.K. Schweitzer, D.D. Starr, The analytical aspects of thorium chemistry, Chem. Rev. 42 (1948) 63–105.
- [3] R. Hussain, K. Luo, Z. Chao, Z. Xiaofeng, Trace elements concentration and distributions in coal and coal mining wastes and their environmental and health impacts in Shaanxi, China. Environ Sci. Pollut. Res. 25 (2018) 19566–19584, https://doi.org/10.1007/s11356-018-2148-2.
- [4] D. Chaudhury, U. Sen, B.K. Sahoo, et al., Thorium promotes lung, liver and kidney damage in BALB/c mouse via alterations in antioxidant systems, Chem. Biol. Interact 363 (2022) 109977, https://doi.org/10.1016/j.cbi.2022.109977.

- [5] R S Kumar, R. Bhaskar, H.K. Sharma, et al., Historical overview and recent progress on supramolecular sensors for thorium recognition, TrAC - Trends Anal Chem. 172 (2024) 117551, https://doi.org/10.1016/j.trac.2024.117551.
- [6] P. Yong, H. Eccles, L.E. Macaskie, Determination of uranium, thorium and lanthanum in mixed solutions using simultaneous spectrophotometry, Anal Chim. Acta 329 (1996) 173–179, https://doi.org/10.1016/j.ccr.2020.213639.
- [7] L. Benedik, A.M. Pilar, H. Prosen, et al., Determination of ultra-trace levels of uranium and thorium in electrolytic copper using radiochemical neutron activation analysis, Appl. Radiat. Isot. 175 (2021) 109801, https://doi.org/10.1016/j. apradiso.2021.109801.
- [8] Daniele Paderni, Luca Giorgi, Vieri Fusi, Mauro Formica, Gianluca Ambrosi, Mauro Micheloni, Chemical sensors for rare earth metal ions, Coordinat. Chem. Rev. 429 (2021) 213639.
- [9] T. Van Acker, S. Theiner, E. Bolea-Fernandez, et al., Inductively coupled plasma mass spectrometry, Nat. Rev. Methods Prim. 3 (2023) 425–461, https://doi.org/ 10.1038/s43586-023-00235-w.
- [10] G.G. El-Gamal, W.I. Mortada, M.M. Hassanien, et al., The selective separation of thorium from uranyl ions using ultrasonic-assisted solidified floating organic drop microextraction, J. Anal. At Spectrom. 36 (2021) 1306–1312.
- [11] R. Selva Kumar, S.K.A. Kumar, K. Vijayakrishna, et al., Development of the Smartphone-Assisted Colorimetric Detection of Thorium by Using New Schiff's Base and Its Applications to Real Time Samples, Inorg. Chem. 57 (2018) 15270–15279, https://doi.org/10.1021/acs.inorgchem.8b02564.
- [12] A.A. Elabd, O.A. Elhefnawy, A new benzeneacetic acid derivative-based sensor for assessing thorium (IV) in aqueous solution based on aggregation caused quenching (ACQ) and aggregation induced emission (AIE), J. Photochem. Photobiol. A Chem. 428 (2022) 113866, https://doi.org/10.1016/j.jphotochem.2022.113866.
- [13] J.P. Desvergne AWC, J.P. Desvergne, A.W. Czarnik, J.P. Desvergne, Chemosensors of ion and molecule recognition, Springer Science & Business Media, 1997.
- [14] A.W. Czarnik, Supramolecular Chemistry, Fluorescence, and Sensing, ACS Publications, 1993.
- [15] S. Paul, P. Barman, N. Dey, M. Watkinson, Recent developments in pyrene-based fluorescence recognition and imaging of Ag+ and Pb2+ ions: Synthesis, applications and challenges, Sensors Diagnost. 3 (2024) 946–967, https://doi.org/ 10.1039/d3sd00289f.
- [16] G. Feng, B. Liu, Aggregation-induced emission (AIE) dots: emerging theranostic nanolights, Acc Chem. Res. 51 (2018) 1404–1414.
- [17] S. Khatkar, G. Thiruppathi, P. Sundararaj, et al., Dehydro acetic acid analogue Schiff base as multimode fluorescence chemosensors for Th4+ and Ni2+ ions and its application to in-vivo bioimaging, J. Photochem. Photobiol. A Chem. 459 (2025) 115999, https://doi.org/10.1016/j.jphotochem.2024.115999.
- [18] B.K. Rani, S.A. John, Pyrene-antipyrine based highly selectIVe and sensitIVe turnon fluorescent sensor for Th(IV), New J. Chem. 41 (2017) 12131–12138, https:// doi.org/10.1039/c7ni01907f.

- [19] R. Selvakumar, S.K. Ashok Kumar, K. Vijayakrishna, et al., Development of highly selective chemosensor for thorium estimation, Sensors Actuators, B Chem. 255 (2017) 1391–1400, https://doi.org/10.1016/j.snb.2017.08.131.
- [20] H. Li, L. Cai, Z. Che, Coumarin-derived fluorescent chemosensors, Adv. Chem. Sensors 1 (2012) 121–150, https://doi.org/10.5772/33157.
- [21] R.S.S. Kumar, S.K.A. Kumar, K. Vijayakrishna, et al., Highly selective CHEF-type chemosensor for lutetium (III) recognition in semi-aqueous media, Spectrochim. Acta Part A Mol. Biomol. Spectrosc. 214 (2019) 32–39, https://doi.org/10.1016/j.ssa.2019.02.003
- [22] S.K. Ramasamy, A. Chinnathambi, S.A. Alharbi, et al., Chelation-enhanced fluorescence-enabled coumarin-hydrazone Schiff bases for the detection of Al3+ ions and its real-time applications, J. Mol. Struct. 1302 (2024) 137411.
- [23] G.L. Long, J.D. Winefordner, Limit of Detection: A Closer Look at the IUPAC Definition, Anal. Chem. 55 (1983) 712A–724A, https://doi.org/10.1021/ ac00258a001.
- [24] P. Job, Formation and stability of inorganic complexes in solution, Ann. di Chim. Appl. 9 (1928) 113–203.
- [25] B.K. Rani, S.A. John, Pyrene–antipyrine based highly selective and sensitive turnon fluorescent sensor for Th (iv), New J. Chem. 41 (2017) 12131–12138.
- [26] A.A. Elabd, O.A. Elhefnawy, A potential sensor for assessing thorium (IV) based on Albuterol sulfate fluorescence enhancement: A density functional theory (DFT) study, Inorg. Chem. Commun. 145 (2022) 110001.
- [27] D. Jothi, S. Manickam, S. Sawminathan, et al., Phenanthridine-based fluorescence sensor for the "off-on" determination of thorium ion and its bio-imaging applications, Dye Pigment 197 (2022) 109826.
- [28] R.S Kumar, S.K. Ashok Kumar, A light activated CMP conjugated 8-aminoquinoline turn-on fluorescent optode for selective determination of Th4+ in an aqueous environment, Dalt Trans. 48 (2019) 12607–12614, https://doi.org/10.1039/ c9dt01830a
- [29] S. Zheng, H. Wang, Q. Hu, et al., Turn-On" fluorescent chemosensor based on B-diketone for detecting Th4+ ions in Aqueous Solution and application in living cell imaging, Sensors Actuat. B Chem. 253 (2017) 766–772, https://doi.org/10.1016/j.spb.2017.06.178.
- [30] A. Dua, P. Saini, S. Goyal, et al., Chromene-chromene Schiff base as a fluorescent chemosensor for Th4+ and its application in bioimaging of Caenorhabditis elegans, Methods 225 (2024) 28–37, https://doi.org/10.1016/j.ymeth.2024.03.002.
- [31] Q. Hu, C. Tang, Y. Yin, et al., AIE and ICT Synergistic Lysosome-Targeted Ratiometric Fluorescence Sensor for the Detection and Imaging of Th4+ in the Liver of Zebrafish and Mice, Anal Chem (2025), https://doi.org/10.1021/acs. analchem.4c06695.
- [32] X. Lin, H. Liang, K. Dai, et al., An Acylhydrazone Fluorescent Sensor: Bifunctional Detection of Thorium (IV) and Vanadyl Ions over Uranyl and Lanthanide Ions, Int J Mol. Sci. 26 (2025), https://doi.org/10.3390/ijms26073231.